18TH WORLD CONFERENCE ON EARTHQUAKE ENGINEERING
WCEE2024
MILAN

MILAN, ITALY
30TH JUNE - 5TH JULY 2024
www.wcee2024.it

SEISMIC PERFORMANCE ENHANCEMENT OF IRREGULAR PLAN BUILDINGS USING BASE ISOLATION TECHNIQUES

A. Kumar[1], A. Menon[2] & A. Meher Prasad[3]

[1] Indian Institute of Technology Madras, Chennai, India, ce22d016@smail.iitm.ac.in

[2] Indian Institute of Technology Madras, Chennai, India

[3] Indian Institute of Technology Madras, Chennai, India

Abstract: *Irregular plan buildings, characterized by variations in floor geometry or mass distribution, have become increasingly popular in modern architectural design. The seismic response of structures is greatly influenced by inherent configuration irregularities, leading to complex dynamic behavior and amplified structural response during seismic events. To enhance the seismic performance of buildings, base isolation has emerged as a popular strategy. The selection of an appropriate isolation device can significantly reduce the structure's engineering demand parameters (e.g., base shear, inter-story drift, floor acceleration, etc.) and disruption caused by earthquakes. The present study investigates the seismic behavior and potential of base isolation techniques in mitigating the amplified structural responses of five-story irregular plan frame buildings supplemented with different base isolation strategies. Typical regular-shaped (RS), cross-shaped (CS), L-shape (LS), and T-shape (TS) building plans are considered for the analysis. Three types of isolation devices commonly adopted in practice, namely (i) Lead rubber bearing (LRB), (ii) Single friction pendulum bearing (SFPB), and (iii) Triple friction pendulum bearing (TFPB), are evaluated for their effectiveness in improving the seismic response of the isolated building model. The modeling and time-history analysis of the base-isolated building is performed using the commercial software SAP2000 with the Fast Nonlinear Analysis solver. The isolation systems are modeled using a two-noded nonlinear link element. The influence of different plan aspect ratios and effective isolation period on the seismic response of the base-isolated building models is investigated. The study demonstrates that base isolation techniques can effectively enhance the dynamic behavior and performance of irregular plan structures in highly seismic-prone regions. Moreover, the analysis results highlight the critical significance of isolator placement and effective isolation period in enhancing seismic performance.*

1 Introduction

The seismic vulnerability of irregular plan buildings has long been a subject of concern in earthquake-prone regions across the globe. As urbanization continues to shape our cities, irregular-plan buildings have become more prevalent in architectural design. Therefore, there is an urgent need for innovative engineering solutions that can enhance their seismic resilience. In recent years, extensive research in earthquake engineering has explored various methods to enhance the seismic performance of structures. Among these methods, base isolation techniques have emerged as a promising solution, demonstrating significant success in mitigating seismic forces in conventional, regularly shaped structures. Over the last five decades, various isolators, including elastomeric and friction types, have been employed effectively in commercial structures [Skinner et

al. (1993)]. In the late 1990s, the Triple Friction Pendulum Bearing (TFPB), a friction-type isolator with three sliding surfaces, was introduced. This innovation, surpassing its predecessor, the Single Friction Pendulum Bearing (SFPB), enhances seismic performance and accommodates larger displacements within a more compact footprint [Fenz and Constantinou (2008)]. Moreover, Constantinou et al. (2011) provide brief and simplified design procedures for elastomeric and friction-type bearings, guiding their utilization in bridges and structures. Regarding the performance assessment of various isolation devices, the literature reports the effectiveness of isolators [Zelleke et al. (2015)]. In seismic design standards, IS 1893 Part-6 (2022) offers essential design guidelines and provisions for base-isolated buildings. Recent studies have explored this topic, such as the Incremental Dynamic Analysis (IDA) conducted by Sabet and Talaeitaba (2022). They investigated regular and irregularly shaped buildings using Lead Rubber Bearing (LRB) and SFPB systems. Additionally, Shadiya and Dilip (2023) performed a seismic time history analysis (THA) on irregularly shaped buildings supplemented using LRB.

Despite extensive research on building structures supplemented with LRB and SFPB, there is a lack of studies comparing their efficacy with the TFPB. Additionally, the existing literature inadequately addresses their application and effectiveness in irregular plan buildings. Therefore, this paper aims to address this research gap by conducting a comprehensive study on the seismic performance enhancement of irregular plan buildings by strategically deploying base isolation techniques. Consequently, this study is structured around two specific objectives: (i) To assess the efficacy of the mentioned base isolation techniques in controlling the seismic response of both regular and irregularly shaped buildings, considering moderate and severe plan irregularities, and (ii) To examine the impact of the effective isolation period on the dynamic behavior and seismic performance of the considered building configurations.

The present study delves into the seismic behavior of five-story reinforced concrete (RC) bare moment-resisting frame building configurations. The analysis encompasses a range of building configurations, including typical regular-shaped (RS) layouts and irregular designs like cross-shaped (CS), L-shape (LS), and T-shape (TS) floor plans. SAP2000 software [SAP2000 (2022)] is used to model and analyse the regular and irregular building models under consideration. Time history analysis (THA) is performed using an ensemble of 30 bi-directional spectrum-scaled acceleration time histories. All the building configurations are assumed to be located in seismic zone V, resting on medium stiff (Type-II) soil as defined by IS 1893 Part-1 (2016). The critical design parameters such as peak story shear, story accelerations, story displacement, and peak in-story drifts are used for comparison and performance evaluation.

Furthermore, several key assumptions have been incorporated to streamline the general structural response analysis of the building models. Firstly, the present study focuses exclusively on irregular buildings with geometric plan irregularity, particularly those with re-entrant corners, in accordance with the guidelines outlined in IS 1893 Part-1 (2016). The soil-structure interaction effects have been excluded from the analysis, with the assumption that all the building models are resting on a robustly designed foundation system. Additionally, the floors within each story are considered rigid diaphragms. Furthermore, the study assumes that the isolated building predominantly demonstrates elastic behavior during seismic events. Lastly, the study excludes vertical seismic effects, deeming them negligible for this investigation.

2 Superstructure Modeling

The present analysis centres on assessing the seismic response of five-story RC building models, encompassing both regular and irregular plan shapes. A square-plan building represents regular structures, while CS, LS, and TS plan buildings are employed to model irregular plan configurations. Additionally, the irregular plan buildings are categorized into moderately irregular (MI) and severely irregular (SI) categories, determined by their projection length-to-plan dimension ratio (as illustrated in Figure 1). In Figure 1, comprehensive details of the models are provided regarding the plan, element cross-section, and elevation of the building models under analysis. All the building models are designed as bare, lateral load-resisting, and moment-resisting RC frames. The building models are assumed to be built with M30 grade concrete and Fe500 grade steel reinforcement. A larger pedestal size of 1×1 meter is incorporated just below the base level in the modeling to account for space requirements related to isolator repair and maintenance. Frame elements are used for modeling beams, columns, and pedestals, while shell elements are used to model slabs within the SAP2000 software.

The imposed dead and live loads applied to the building model conform to IS 875 Part-1 (1987) and IS 875 Part-2 (1987). The building models account for the self-weight of concrete (25 kN/m^3) and masonry (20 kN/m^3), as well as the specified thicknesses of exterior walls (230 mm) and interior walls (115 mm). Additionally, the model considers a 125 mm thick slab with imposed loads of 3 kN/m^2 on the floors and 0.75 kN/m^2 on the roof, assuming no access. Moreover, it incorporates provisions for story finishes (1 kN/m^2) and roof treatments (1.5 kN/m^2). The total weight of the RS building models is 70,308 kN, with a corresponding seismic weight of 60,900 kN. For the irregular plan building models considered, namely MI and SI, the total weight is 50,548 kN and 85,713 kN, whereas the seismic weight of the MI and SI building models is 44,212 kN and 74,769 kN, respectively. Note that the analysis excludes the weight of isolators, as it constitutes a negligible fraction (approximately 1%) compared to the total weight of the entire building model.

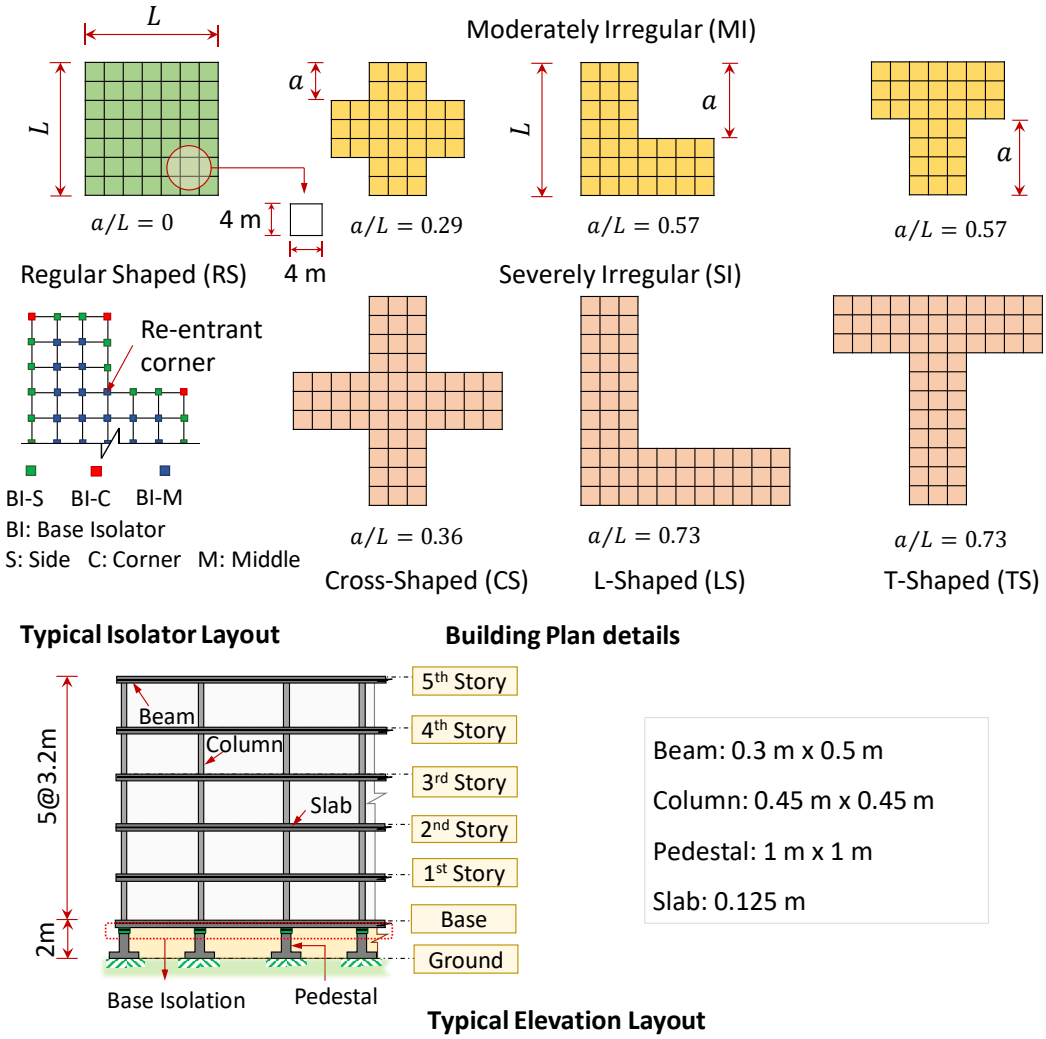

Figure 1. Building models plan, elevation, and element cross-section details.

3 Base Isolator Modeling

The design methodology for the analysed isolators, namely the LRB, SFPB, and TFPB, is derived from Constantinou et al. (2011) and IS 1893 Part-6 (2022). As the selected isolators demonstrate nonlinear behavior, a two-noded nonlinear isolator link element within SAP2000 is deployed to accurately model the base isolators for the present study. Specifically, the LRB, SFPB, and TFPB isolators are modeled using the Rubber isolator, Friction isolator, and Triple pendulum isolator link elements, respectively [SAP2000 (2022)]. The upper-bound properties of the isolators are considered in the design and analysis. The isolators are designed to accommodate three isolation periods: 2, 2.5, and 3 seconds. The effective damping ratio of the designed isolators ($\xi_{eff} = 30\ \%$) remains consistent across all the isolators under study. Table 1 presents a

comprehensive summary of the designed isolator link properties, with notations and terminology conforming to the conventions established by Constantinou et al. (2011). In alignment with the axial load capacities within various locations in the building plan, encompassing both regular and irregular building models, the base isolators (BI) in this study are categorized as BI-C (corner), BI-S (side/periphery other than corners), and BI-M (interior/middle) at the base level. Additionally, as illustrated in Figure 1, the BI-C, BI-S, and BI-M isolators exhibit designed axial load capacities of 650 kN, 850 kN, and 1050 kN, respectively.

Table 1. Summary of designed isolator link properties.

Isolator/Category		**BI-C**			**BI-S**			**BI-M**		
	T_{eff} **(s)**	**2**	**2.5**	**3**	**2**	**2.5**	**3**	**2**	**2.5**	**3**
LRB	D_m (mm)	150	187	224	150	187	224	150	187	224
	Q (kN)	46	37	31	60	48	40	75	60	50
	$k_{initial}$ (kN/m)	2989	1913	1329	3909	2502	1737	4829	3091	2146
	n	0.10	0.10	0.10	0.10	0.10	0.10	0.10	0.10	0.10
	k_{eff} (kN/m)	654	419	291	855	547	380	1056	676	470
	c_{eff} (kN-s/m)	125	100	83	163	131	109	202	161	135
SFPB	D_m (mm)	150	187	224	150	187	224	150	187	224
	R_{eff} (mm)	1878	2935	4227	1878	2935	4227	1878	2935	4227
	$k_{initial}$ (kN/m)	40737	32484	27012	53271	42479	35323	65806	52475	43634
	μ_{slow}	0.0311	0.0248	0.0207	0.0311	0.0248	0.0207	0.0311	0.0248	0.0207
	μ_{fast}	0.0621	0.0496	0.0413	0.0621	0.0496	0.0413	0.0621	0.0496	0.0413
	k_{eff} (kN/m)	654	419	291	855	547	380	1056	676	470
	c_{eff} (kN-s/m)	125	100	83	163	131	109	202	161	135
	r (s/m)	50	50	50	50	50	50	50	50	50
TFPB	D_m (mm)	242	262	300	242	262	300	242	262	300
	k_{eff} (kN/m)	654	419	291	855	547	380	1056	676	470
	c_{eff} (kN-s/m)	125	100	83	163	131	109	202	161	135
	$k_{initial,1}$ (kN/m)	2702	1979	1233	3534	2588	1613	4365	3197	1992
	$\mu_{slow,1}$	0.0236	0.0178	0.0155	0.0236	0.0178	0.0155	0.0236	0.0178	0.0155
	$\mu_{fast,1}$	0.0471	0.0356	0.0310	0.0471	0.0356	0.0310	0.0471	0.0356	0.0310
	$R_{eff,1}$ (mm)	1158	1727	2578	1158	1727	2578	1158	1727	2578
	$d_{Stop,1}$ (mm)	156	178	209	155	178	209	154	178	209
	$k_{initial,2}$ (kN/m)	582	531	374	761	695	489	940	858	604
	$\mu_{slow,2}$	0.0051	0.0048	0.0047	0.0051	0.0048	0.0047	0.0051	0.0048	0.0047
	$\mu_{fast,2}$	0.0102	0.0095	0.0094	0.0102	0.0095	0.0094	0.0102	0.0095	0.0094
	$R_{eff,2}$ (mm)	307	449	756	307	449	756	307	449	756
	$d_{Stop,2}$ (mm)	23	23	33	23	23	33	23	23	33
	r (s/m)	50	50	50	50	50	50	50	50	50

4 Ground Motion Selection

This study employs bi-directional time histories to assess the dynamic behavior of the models under consideration. An ensemble of 30 ground motions is downloaded from the Pacific Earthquake Engineering Research Centre (PEER) NGA West database, accessible at https://ngawest2.berkeley.edu/. The selected ensemble covers a range of earthquake magnitudes (M_w) from 6.5 to 7.5 and distances from the fault rupture (R_{rup}) spanning 20 km to 80 km. The earthquake records are chosen explicitly from sites with average shear wave velocities (V_{s30}) ranging from 300 m/s to 600 m/s, aligning with medium stiff soil conditions. Ground acceleration histories for the analysis are generated using a spectrum scaling technique to scale the bi-directional records to the Indian standard (IS) code design spectrum [IS 1893 Part-1 (2016)]. The present analysis employs the design spectrum corresponding to zone V and medium stiff (Type-II) soil conditions. The scaling factors applied to the ground motion records vary between 0.6 and 3.06. Figure 2 illustrates the

Maximum Considerable Earthquake (MCE) response spectra for the *x*-direction and *y*-direction, alongside the mean spectrum derived from the ensemble of 30 bi-directional time histories and the IS target spectrum.

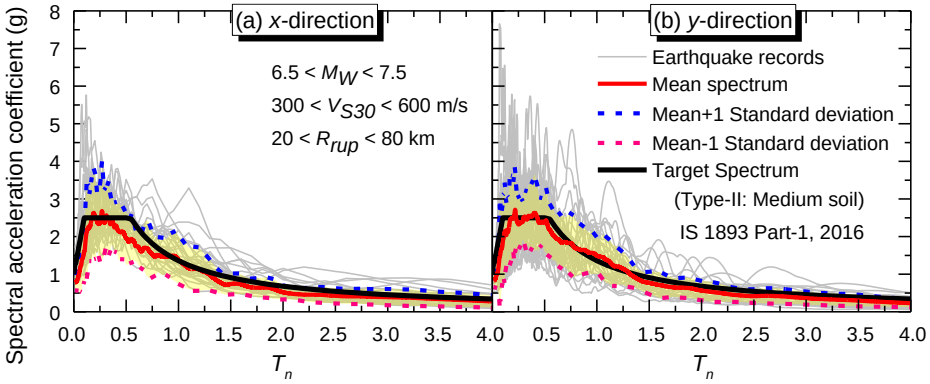

Figure 2. Maximum Considerable Earthquake (MCE) response spectra curves in the (a) x-direction and (b) y-direction, alongside the mean spectrum of the ground motion ensemble and IS target spectrum.

5 Modal Analysis

The modal analysis is conducted using Ritz vectors, encompassing 350 modes and accounting for a mass source that included 100% dead load and 25% typical story live load, with the live roof load excluded [as per IS 1893 Part-1 (2016)]. A constant damping ratio of 5% is assumed for the fixed base model; however, for the isolated models, a damping override of 0% is defined for the first three isolator modes, while a constant damping ratio of 5% is defined for the remaining modes. Figure 3 illustrates the modal behavior of different plan shapes for the isolated building configurations considered in the study, highlighting the first three modes: transitional modes in the *x*-and *y*-directions, along with a rotational mode.

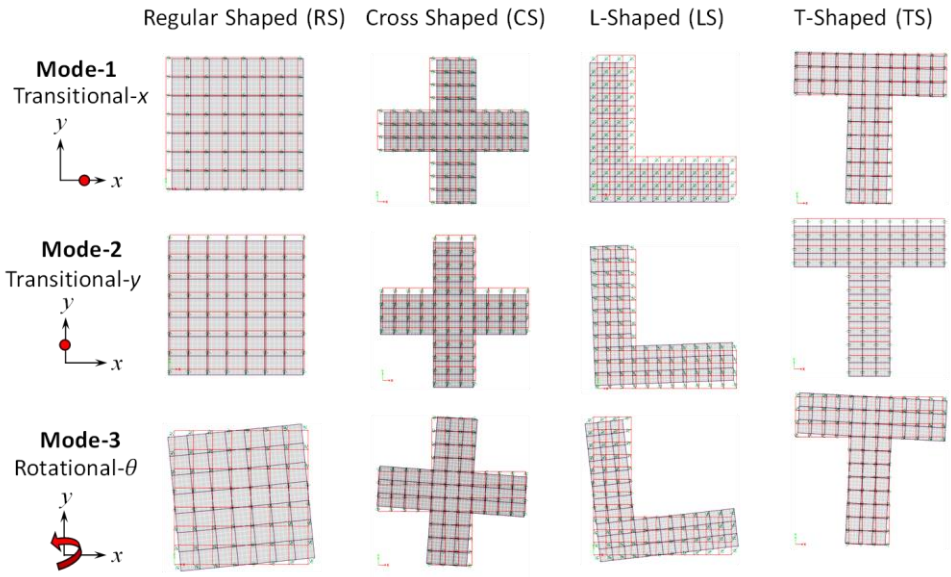

Figure 3. Modal behavior of RS, CS, LS, and TS isolated building configurations: first three modes, including transitional modes in x-and y-directions, and rotational mode.

In a complementary fashion, Table 2 presents comprehensive information on the translational periods, mass participation ratios, and a rotational mode for the building models under consideration. This data is provided for both fixed and isolated conditions, with effective isolation periods of 2, 2.5, and 3 seconds explored across considered configurations of the buildings. Notably, in the case of base-isolated models, more than 96% of the mass is actively involved in the first fundamental mode in both orthogonal directions. It observed that for Irregular building models, the transitional period in the *x*-direction is slightly higher than in the *y*-direction. Further, the fundamental period is slightly longer for the SI building configurations than for MI configurations.

Table 2. Translational and rotational periods and their respective modal mass participation ratios for fixed and isolated building models with different effective isolation periods.

Model isolated with:			LRB			SFPB			TFPB		
		Fixed	T_{eff} (s)			T_{eff} (s)			T_{eff} (s)		
			2	2.5	3	2	2.5	3	2	2.5	3
Regular	T_x (s)	0.689	2.057	2.527	3.002	2.057	2.527	3.002	2.057	2.527	3.002
	Γ_x (%)	67.58	96.21	95.56	96.20	94.67	96.66	93.90	95.77	95.62	95.74
	T_y (s)	0.689	2.057	2.527	3.002	2.057	2.527	3.002	2.057	2.527	3.002
	Γ_y (%)	67.58	96.21	95.56	96.20	94.67	96.66	93.90	95.77	95.62	95.74
	T_θ (s)	0.659	2.036	2.504	2.978	2.036	2.504	2.978	2.036	2.504	2.978
	Γ_θ (%)	0.00	0.00	0.00	0.00	0.00	0.00	0.00	0.00	0.00	0.00
CS-MI	T_x (s)	0.690	2.061	2.531	3.006	2.061	2.531	3.006	2.061	2.531	3.006
	Γ_x (%)	50.36	62.59	63.84	67.73	65.42	81.2	77.87	74.24	71.37	69.93
	T_y (s)	0.690	2.061	2.531	3.006	2.061	2.531	3.006	2.061	2.531	3.006
	Γ_y (%)	50.36	62.59	63.84	67.73	65.42	81.2	77.87	74.24	71.37	69.93
	T_θ (s)	0.663	2.033	2.499	2.971	2.033	2.499	2.971	2.033	2.499	2.971
	Γ_θ (%)	0.00	0.00	0.00	0.00	0.00	0.00	0.00	0.00	0.00	0.00
CS-SI	T_x (s)	0.690	2.061	2.531	3.007	2.061	2.531	3.007	2.061	2.531	3.007
	Γ_x (%)	53.93	78.18	66.51	70.86	79.61	67.96	77.21	70.1	71.67	66.99
	T_y (s)	0.690	2.061	2.531	3.007	2.061	2.531	3.007	2.061	2.531	3.007
	Γ_y (%)	53.93	78.18	66.51	70.86	79.61	67.96	77.21	70.10	71.67	66.99
	T_θ (s)	0.682	2.050	2.517	2.990	2.050	2.517	2.990	2.050	2.517	2.990
	Γ_θ (%)	0.00	0.00	0.00	0.00	0.00	0.00	0.00	0.00	0.00	0.00
LS-MI	T_x (s)	0.693	2.057	2.525	3.000	2.057	2.525	3.000	2.057	2.525	3.000
	Γ_x (%)	31.29	54.63	65.98	70.85	54.63	65.98	70.85	54.63	65.98	70.85
	T_y (s)	0.690	2.052	2.520	2.993	2.052	2.520	2.993	2.052	2.520	2.993
	Γ_y (%)	35.01	59.55	73.56	80.21	59.55	73.56	80.21	59.55	73.56	80.21
	T_θ (s)	0.663	2.018	2.478	2.944	2.018	2.478	2.944	2.018	2.478	2.944
	Γ_θ (%)	3.72	3.22	2.30	1.87	3.22	2.3	1.87	3.22	2.30	1.87
LS-SI	T_x (s)	0.701	2.066	2.534	3.008	2.066	2.534	3.008	2.066	2.534	3.008
	Γ_x (%)	22.09	36.15	40.65	43.90	36.15	40.65	43.90	36.15	40.65	43.90
	T_y (s)	0.690	2.061	2.531	3.007	2.061	2.531	3.007	2.061	2.531	3.007
	Γ_y (%)	35.05	48.69	48.77	48.81	48.69	48.77	48.81	48.69	48.77	48.81
	T_θ (s)	0.671	2.049	2.519	2.994	2.049	2.519	2.994	2.049	2.519	2.994
	Γ_θ (%)	12.97	12.53	8.12	4.90	12.53	8.13	4.90	12.53	8.13	4.90
TS-MI	T_x (s)	0.691	2.062	2.531	3.006	2.062	2.531	3.006	2.062	2.531	3.006
	Γ_x (%)	65.97	96.15	97.03	97.38	96.15	97.03	97.38	96.15	97.03	97.38
	T_y (s)	0.690	2.061	2.531	3.006	2.061	2.531	3.006	2.061	2.531	3.006
	Γ_y (%)	70.03	97.34	97.51	97.58	97.34	97.51	97.58	97.34	97.51	97.58
	T_θ (s)	0.663	2.036	2.503	2.975	2.036	2.503	2.975	2.036	2.503	2.975
	Γ_θ (%)	4.06	1.19	0.48	0.20	1.19	0.48	0.20	1.19	0.48	0.20
TS-SI	T_x (s)	0.698	2.064	2.533	3.008	2.064	2.533	3.008	2.064	2.533	3.008
	Γ_x (%)	46.54	80.02	88.41	92.89	80.02	88.41	92.89	80.02	88.41	92.89
	T_y (s)	0.690	2.061	2.531	3.007	2.061	2.531	3.007	2.061	2.531	3.007
	Γ_y (%)	70.11	97.38	97.55	97.61	97.38	97.55	97.61	97.38	97.55	97.61
	T_θ (s)	0.675	2.050	2.519	2.993	2.050	2.519	2.993	2.050	2.519	2.993
	Γ_θ (%)	23.56	17.35	9.14	4.73	17.36	9.14	4.73	17.36	9.14	4.73
		$T_{x,y\ and\ \theta}$ = Natural period				$\Gamma_{x,y\ and\ \theta}$ = Mass participation ratio					

Interestingly, RS and CS buildings have shorter fundamental periods than LS and TS buildings in two orthogonal directions. Additionally, RS and CS buildings have higher mass participation ratios in translational modes when compared to TS and LS buildings. RS and CS buildings typically show zero mass participation in rotational modes. In the *y*-direction, LS and TS buildings exhibit higher mass participation in translational modes with shorter fundamental periods. It is worth noting that LS and TS buildings can also manifest torsional motion in their initial translational modes, as depicted in Figure 3. A ground motion with significant rotational characteristics can trigger torsional responses in these buildings. Moreover, the modal analysis also underscores the effect of longer effective isolation periods, revealing that longer effective isolation periods reduce mass participation in rotational modes and increase mass participation in translational modes for TS and LS buildings. Consequently, it mitigates the torsional response of the buildings.

6 Time History Analysis

In the following investigation, THA employs SAP2000 as the analysis software, utilizing a Fast Nonlinear Analysis (FNA) solver. To initiate the analysis, dead and live loads as per the superstructure modeling section are applied, followed by the definition of a nonlinear gravity step employing a ramp function. This step serves as the initial condition for the FNA solver. Seismic response assessment is performed using an ensemble of 30 bi-directional spectrum-scaled ground motion records. The analysis results are reported in terms of average peak responses. Critical response parameters such as story shear, story acceleration, story displacement, and inter-story drift are monitored in the two orthogonal directions to evaluate average peak responses. Figure 4 shows a descriptive plot illustrating the average peak responses of fixed and isolated RS building models along the two orthogonal directions. Note that the plots display story shear response in terms of seismic shear coefficient normalized with respect to the seismic weights of the building models.

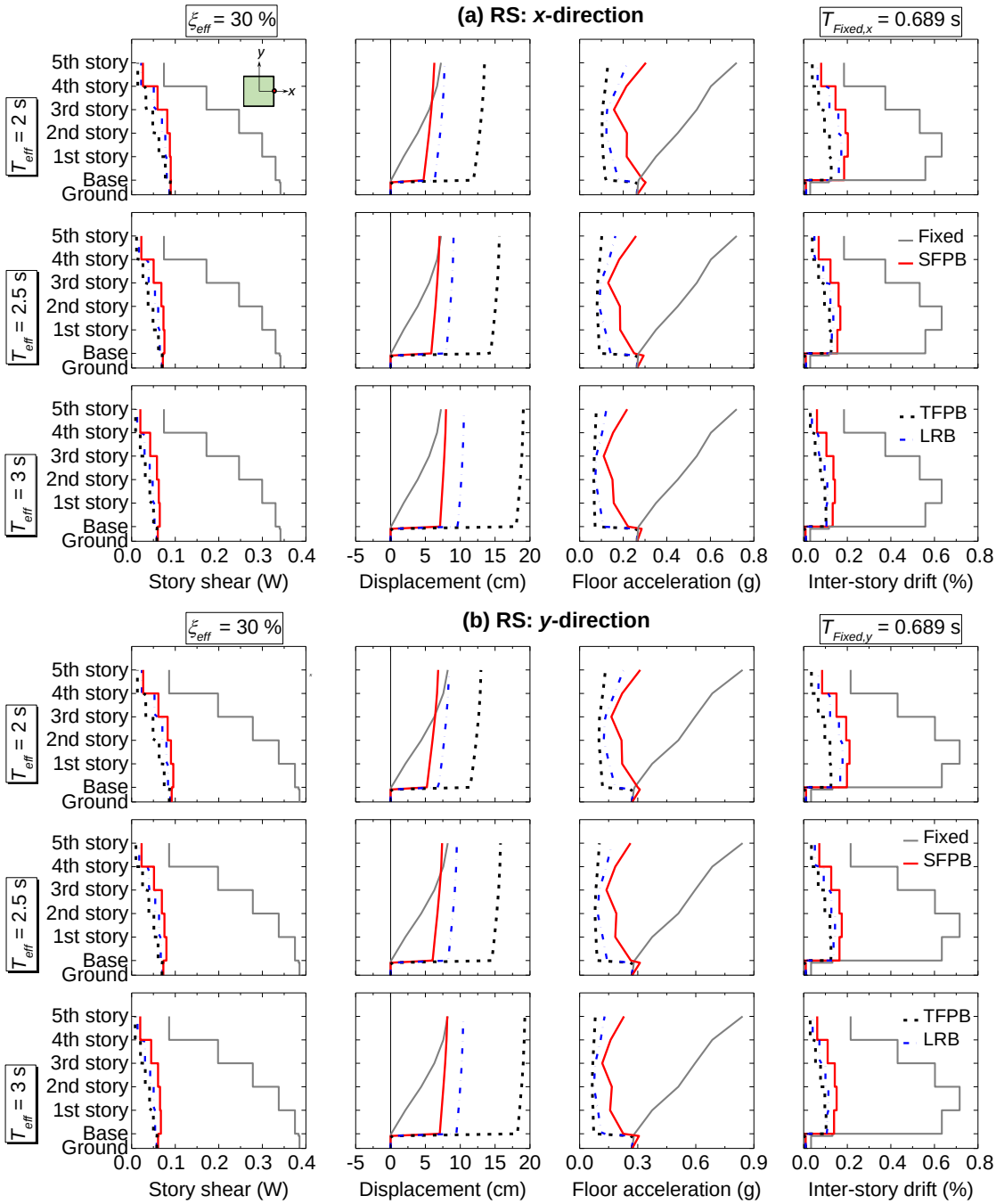

Figure 4. Average peak seismic responses of RS-fixed and isolated building models along (a) x-direction and (b) y-direction.

Furthermore, Figures 5 through 7 present plots for CS, LS, and TS buildings featuring MI and SI configurations. These plots for irregular building configurations exclusively present the average peak response along the *x*-direction, as the responses in the *y*-direction exhibit a similar trend.

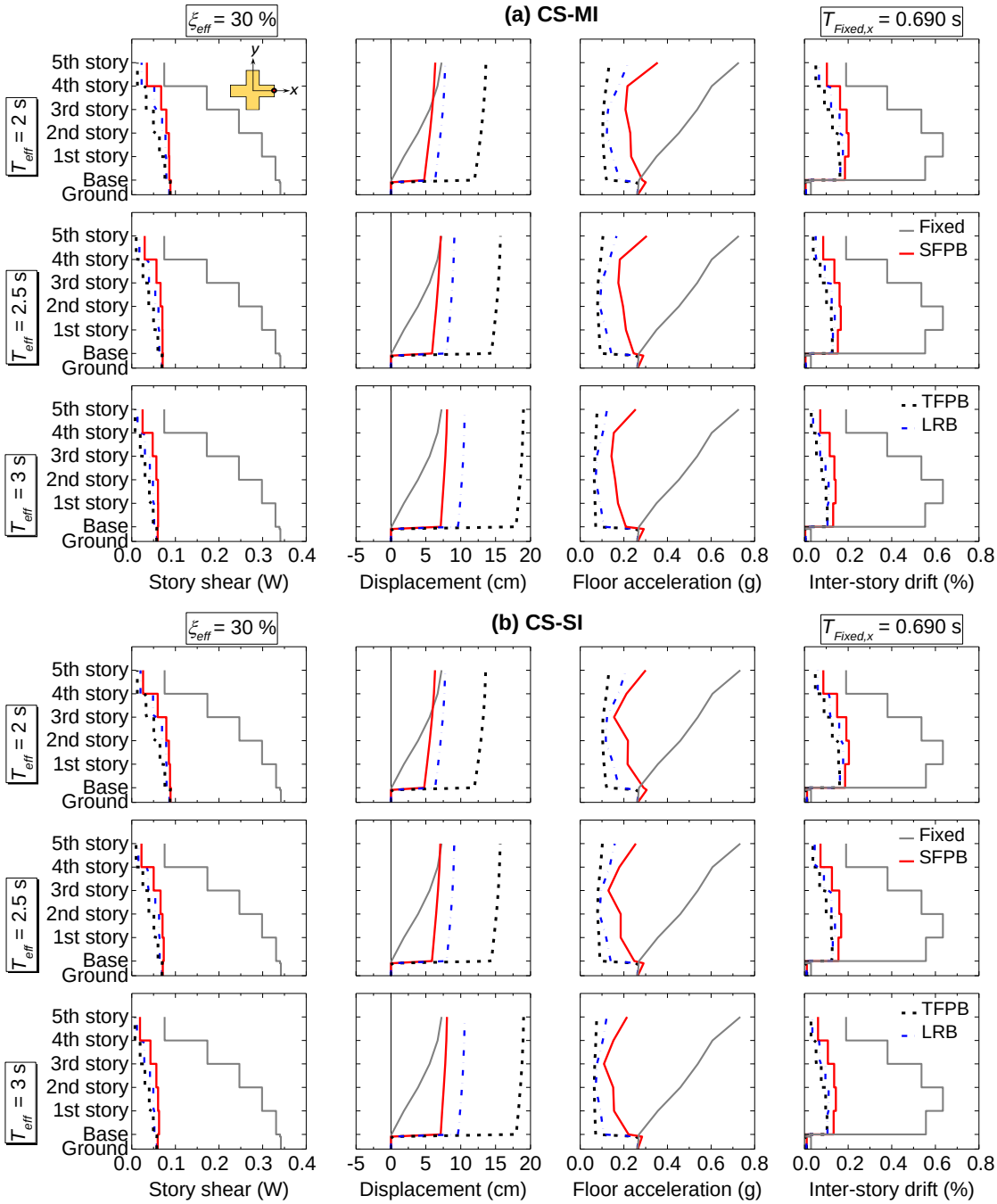

Figure 5. Average peak seismic responses of CS-fixed and isolated building models for (a) MI and (b) SI configurations.

In the context of seismic responses, LS building configurations exhibit higher seismic responses followed by TS, CS, and the least in RS buildings. Among irregular buildings, SI building configurations show slightly higher responses than MI building configurations. Nevertheless, the reduction in seismic responses remains consistent across all building configurations. Notably, TFPB isolators consistently lead to higher reductions in story shear, story acceleration, and inter-story drift, followed by LRB, with SFPB exhibiting the least reduction. However, TFPB demands higher displacements at the isolator level as compared to LRB and SFPB isolators. Notably, SFPB isolators consistently show the least isolator displacement demand.

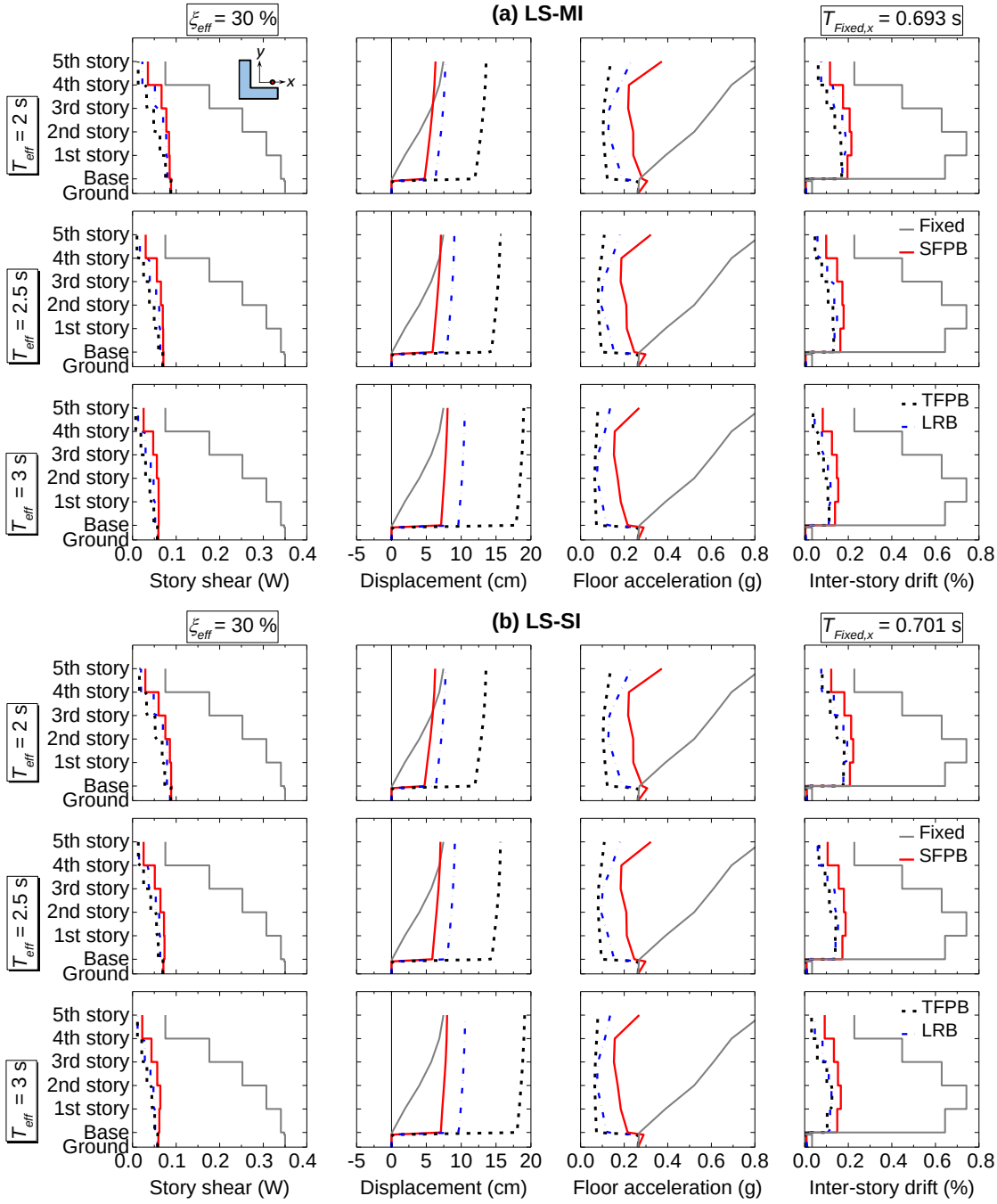

Figure 6. Average peak seismic responses of LS-fixed and isolated building models for (a) MI and (b) SI configurations.

Additionally, representative isolators from extreme corners, re-entrant corners/sides, and the interior have been selected to demonstrate the effect of isolator location on the hysteretic behavior of isolators. Figure 8 illustrates a representative hysteresis plot for the Iwate Japan (2008) earthquake time history scaled with a factor of 0.85, chosen for its maximum seismic responses. This plot characterizes the hysteretic behavior of isolators with a 3-second effective isolation period, explicitly focusing on SI configurations of irregular building configurations as a worst-case scenario. The analysis highlights several key findings: LRB isolators exhibit minimal sensitivity to building configurations and locations. In comparison, SFPB and TFPB isolators are notably more responsive to specific locations within the building configurations. Corner isolators consistently experience higher lateral forces and displacements than peripheral and central isolators, attributed to torsional effects during seismic events. Caution is warranted, as isolators at outer and re-entrant corners may exceed their designed shear capacity if torsional motion effects are not appropriately addressed in structural design

and assessment. These findings emphasize the importance of considering isolator location in building plans when designing and assessing base isolators for seismic resilience, especially friction-type isolators.

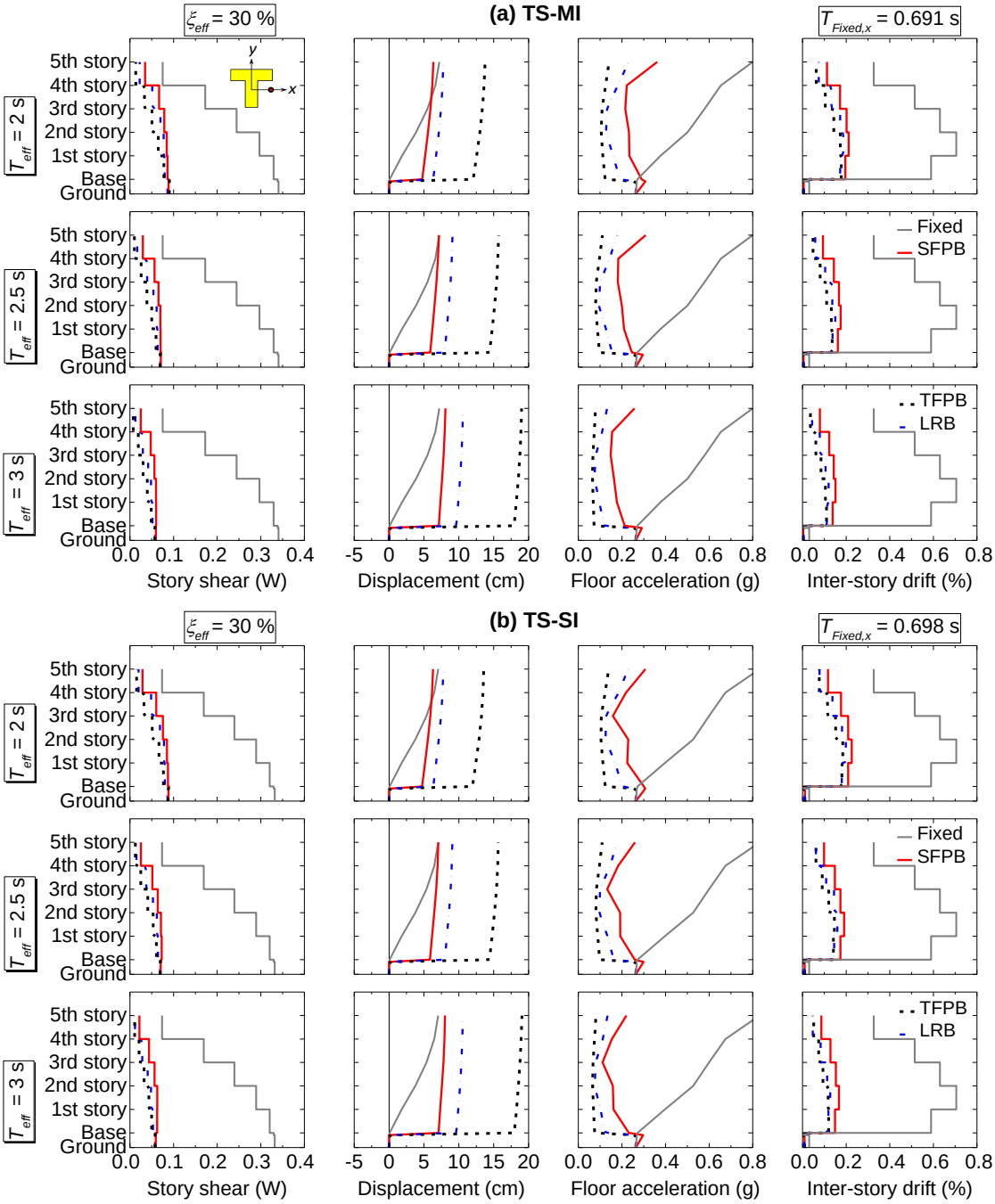

Figure 7. Average peak seismic responses of TS-fixed and isolated building models for (a) MI and (b) SI configurations.

Moreover, Table 3 showcases the effectiveness of the base isolation devices deployed and the impact of varying effective isolation periods on the seismic response control of RC building models under consideration. The assessment of base isolation effectiveness is quantified in terms of percentage reduction in the seismic response quantities with respect to the fixed base configurations. Table 3 displays combined average percentage reductions in seismic responses (in both *x*-and *y*-directions) to assess overall isolation system effectiveness. These reductions are reported for RS buildings and include MI and SI configurations. The MI and SI configurations include averages from LS, CS, and TS buildings, as the analysis shows that plan shape minimally impacts seismic response reduction. The table demonstrates that the use of seismic isolators significantly enhances the overall seismic performance across all configurations.

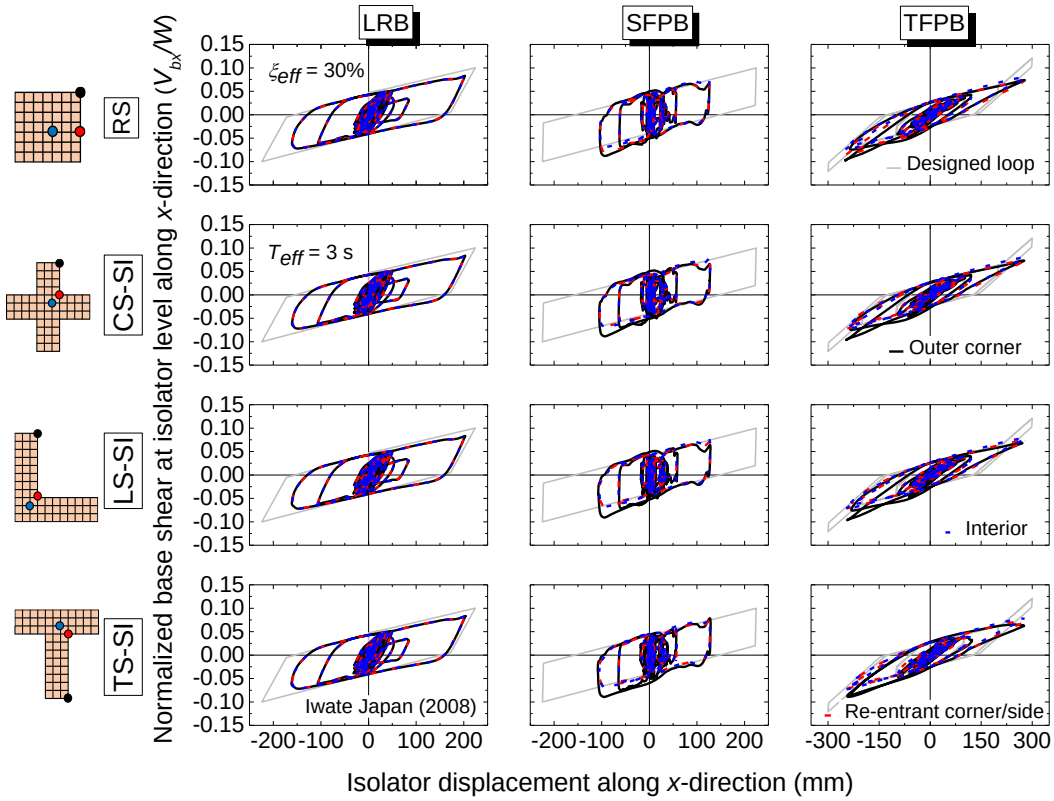

Figure 8. Representative hysteretic response of isolators at different locations within the buildings with different shapes along the x-direction for Iwate Japan (2008) earthquake.

Table 3. Average reductions in seismic responses for different isolator types and effective isolation periods.

T_{eff} (s)		2			2.5			3		
Isolator Type	**Configuration**	**SFPB**	**LRB**	**TFPB**	**SFPB**	**LRB**	**TFPB**	**SFPB**	**LRB**	**TFPB**
Average Reduction in Story Shear (%)	RS	71	74	79	76	80	84	80	84	87
	MI	69	74	80	75	80	84	78	84	87
	SI	70	75	79	76	80	83	79	84	86
Average Reduction in Story Acceleration (%)	RS	48	65	75	55	73	81	62	79	85
	MI	45	65	76	53	73	81	60	79	85
	SI	48	65	76	55	73	81	62	79	85
Average Reduction in Inter-Story Drift (%)	RS	65	71	82	71	77	82	75	82	85
	MI	64	72	76	70	78	81	74	83	85
	SI	64	72	75	70	78	80	74	82	85

The analysis reveals that, on average, the RS building configuration exhibits a slightly higher percentage reduction in seismic response than the MI and SI building configurations. Furthermore, the reduction in story shear stands out as the most prominent, followed by inter-story drift and story acceleration reductions. These trends vary noticeably depending on the isolator type and effective isolation period. Notably, all isolators demonstrate significant effectiveness in mitigating the seismic response of the building configurations. The isolators under investigation, namely SFPB, LRB, and TFPB, consistently deliver significant reductions in critical seismic response quantities, with average reductions ranging from 70% to 87% for story shear, 47% to 85% for story acceleration, and 64% to 85% for inter-story drift. It is worth highlighting that the use of TFPB isolators results in a notably higher reduction in seismic response when compared to other isolators used in the study. However, the building models isolated with TFPB experience higher displacements at the isolator level. Nevertheless, TFPB isolators demonstrate noteworthy effectiveness in controlling inter-story drifts and achieving the desired seismic performance within the linear elastic range. Additionally, the inter-story drift values observed in the isolated building models consistently remain below the threshold of 0.4%, ensuring the isolated structure's elastic performance during earthquakes. In relation to the effective isolation period, it is

evident from the study that increasing the effective isolation period leads to better seismic performance and response control. These findings emphasize the significance of judiciously choosing isolator types for desired structural performance and optimizing the effective isolation period to improve the overall effectiveness of base isolation techniques in seismic design.

7 Conclusion

In this comprehensive study, dynamic behavior and the seismic performance of five-story RC moment-resisting frame buildings were thoroughly explored. The study encompasses regular and irregular building configurations with moderate and severe irregularities, supplemented with LRB, SFPB, and TFPB isolators. Furthermore, the influence of the isolator's effective period on the seismic response of these base-isolated building models has been closely examined. The following conclusions are drawn from an extensive analysis of the results and the observed trends:

1. Base isolation devices demonstrate their effectiveness irrespective of regular and irregular plan building configurations. Notably, the TFPB isolator outperforms SFPB and LRB isolators in reducing in-story drift, story shear, and story acceleration.
2. The studied isolators (SFPB, LRB, and TFPB) consistently reduce critical seismic responses significantly, including story shear (70% to 87%), story acceleration (47% to 85%), and inter-story drift (64% to 85%).
3. When using friction-type isolators, the placement within the building plan, especially at outer and re-entrant corners, significantly influences their performance, emphasizing the importance of careful design and analysis for safety in design.
4. Increasing effective isolation periods from 2 to 3 seconds yields higher reductions in critical seismic responses across all isolator types, with minimal increases in isolator-level displacement demand.
5. Proper selection of isolator types and optimization of isolation periods are crucial for enhancing the overall effectiveness of base isolation systems in seismic design.

8 References

Constantinou, M. C., Kalpakidis, I., Filiatrault, A., and Lay, R. A. E. (2011). LRFD-Based Analysis and Design Procedures for Bridge Bearings and Seismic Isolators. In *MCEER*: Vol. MCEER-11-0 (Issue 65).

Fenz, D. M., and Constantinou, M. C. (2008). Modeling triple friction pendulum bearings for response-history analysis. *Earthquake Spectra*, 24(4).

IS 875 Part-1 (1987). IS 875-1: Code of Practice for Design Loads (Other Than Earthquake) For Buildings and Structures, Part 1: Dead Loads. *Bureau of Indian Standards*, New Delhi.

IS 875 Part-2 (1987). IS 875-2: Code of Practice for Design Loads (Other than Earthquake) for Buildings and Structures, Part 2: Imposed Loads. *Bureau of Indian Standards*, New Delhi.

IS 1893 Part-1 (2016). IS 1893-1: Criteria for Earthquake resistant design of structures, Part 1: General Provisions and buildings. *Bureau of Indian Standards*, New Delhi.

IS 1893 Part-6 (2022). IS 1893-6: Criteria for Earthquake resistant design of structures, Part 6: Base Isolated Buildings. *Bureau of Indian Standards*, New Delhi.

Shadiya, P. V., and Dilip, P. P. (2023). Seismic Analysis of Irregular Buildings with And Without Lead Plug Rubber Bearings (LPRB). *Journal of Recent Activities in Infrastructure Science*, 8(2).

Skinner, R. I., Robinson, W. H. and McVerry, G. H. (1993). An Introduction to Seismic Isolation, New York: *John Wiley & Sons Inc*.

SAP2000 (2022). CSI Spain | *Computers and Structures Inc*. In SAP 2000.

Sabet, B., and Talaeitaba, S. B. (2022). IDA analysis of regular and irregular seismically isolated structures in different stories and different seismic categories. *Structures*, 43.

Zelleke, D. H., Elias, S., Matsagar, V. A., and Jain, A. K. (2015). Supplemental dampers in base-isolated buildings to mitigate large isolator displacement under earthquake excitations. *Bulletin of the New Zealand Society for Earthquake Engineering*, 48(2).